

Published in final edited form as:

J Proteome Res. 2021 February 05; 20(2): 1424–1433. doi:10.1021/acs.jproteome.0c00830.

Functionally Integrated Top-Down Proteomics for Standardized Assessment of Human Induced Pluripotent Stem Cell-Derived Engineered Cardiac Tissues

Jake A. Melby,

Department of Chemistry, University of Wisconsin–Madison, Madison, Wisconsin 53706, United States

Willem J. de Lange,

Department of Pediatrics, University of Wisconsin–Madison, Madison, Wisconsin 53705, United States

Jianhua Zhang,

Department of Medicine, University of Wisconsin-Madison, Madison, Wisconsin 53705, United States

David S. Roberts,

Department of Chemistry, University of Wisconsin–Madison, Madison, Wisconsin 53706, United States

Stanford D. Mitchell.

Department of Cell and Regenerative Biology, University of Wisconsin–Madison, Madison, Wisconsin 53705, United States

Trisha Tucholski,

Department of Chemistry, University of Wisconsin–Madison, Madison, Wisconsin 53706, United States

Gina Kim,

Corresponding Authors J. Carter Ralphe, jcralphe@pediatrics.wisc.edu; Phone: 608-262-1603; Ying Ge, Phone: 608-265-4744; ying.ge@wisc.edu.

The authors declare the following competing financial interest(s): T.J.K. is a consultant for Cellular Dynamics International. The other authors declare no conflict of interest. The mass spectrometry-based proteomics data have been deposited to the ProteomeXchange Consortium under accession PXD022814.

Supporting Information

The Supporting Information is available free of charge at https://pubs.acs.org/doi/10.1021/acs.jproteome.0c00830.

Supplementary Methods: SDS-polyacrylamide gel electrophoresis (SDS-PAGE); Supplementary Figure S1: Workflow of integrated functional assessment and top-down proteomics method for analysis of hiPSC-ECT; Supplementary Figure S2: SDS-PAGE of HEPES/TFA extracts from Day 23 and Day 51 hiPSC-ECT samples; Supplementary Figure S3: Three injection replicates demonstrate high reproducibility of protein separation and instrument performance of a Day 23 hiPSC-ECT; Supplementary Figure S4: Three injection replicates demonstrate high reproducibility of protein separation and instrument performance of a Day 51 hiPSC-ECT; Supplementary Figure S5: Comparison of key myofilament proteins in the hiPSC-ECT samples using top-down LC-MS/MS method; Supplementary Figure S6: Online LC-MS/MS of MLC1 ventricular and atrial isoforms; Supplementary Figure S7: Comparison of the ventricular and atrial isoforms of myosin light chain 1 between the Day 23 and Day 51 hiPSC-ECTs; Supplementary Figure S8: Representative deconvoluted spectra of major sarcomeric proteins found in the Day 23 and Day 51 hiPSC-ECTs; Supplementary Figure S9: Deconvoluted mass spectra of sarcomeric proteoforms; Supplementary Figure S10: Comparison of the slow skeletal and cardiac troponin I isoforms between the Day 23 and Day 51 hiPSC-ECTs; Supplementary Figure S11: Integrated functional assessments with cTnT6 and cTnI phosphorylation levels; Supplementary Figure S12: Integrated functional assessments with α -Tpm, cTnT6, and cTnI phosphorylation levels normalized for the effect of time in 3D hiPSC-ECT culture (PDF)

Department of Medicine, University of Wisconsin–Madison, Madison, Wisconsin 53705, United States

Andreas Kyrvasilis,

Department of Cell and Regenerative Biology, University of Wisconsin–Madison, Madison, Wisconsin 53705, United States

Sean J. McIlwain,

Department of Biostatistics and Medical Informatics and UW Carbone Cancer Center, School of Medicine and Public Health, University of Wisconsin–Madison, Madison, Wisconsin 53705, United States

Timothy J. Kamp,

Department of Cell and Regenerative Biology and Department of Medicine, University of Wisconsin–Madison, Madison, Wisconsin 53705, United States

J. Carter Ralphe,

Department of Pediatrics, University of Wisconsin–Madison, Madison, Wisconsin 53705, United States

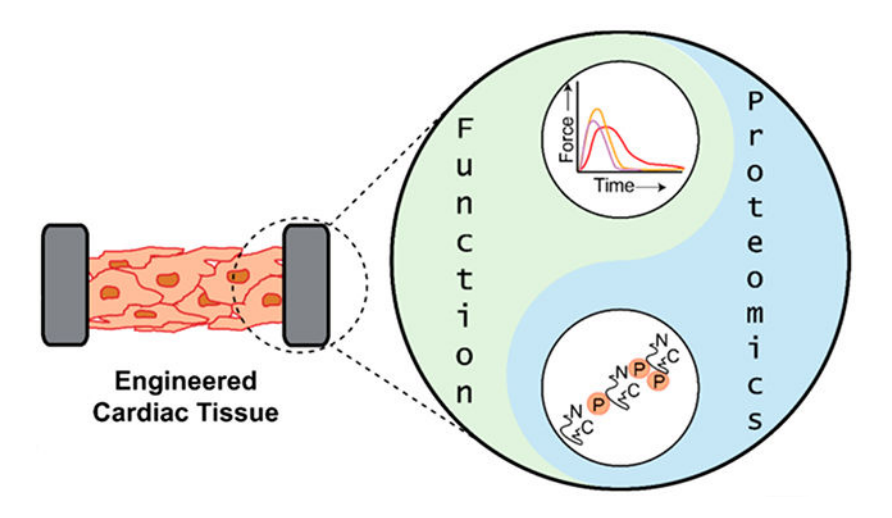
Ying Ge

Department of Chemistry, Department of Cell and Regenerative Biology, and Human Proteomics Program, University of Wisconsin–Madison, Madison, Wisconsin 53706, United States

Abstract

Three-dimensional (3D) human induced pluripotent stem cell-derived engineered cardiac tissues (hiPSC-ECTs) have emerged as a promising alternative to two-dimensional hiPSC-cardiomyocyte monolayer systems because hiPSC-ECTs are a closer representation of endogenous cardiac tissues and more faithfully reflect the relevant cardiac pathophysiology. The ability to perform functional and molecular assessments using the same hiPSC-ECT construct would allow for more reliable correlation between observed functional performance and underlying molecular events, and thus is critically needed. Herein, for the first time, we have established an integrated method that permits sequential assessment of functional properties and top-down proteomics from the same single hiPSC-ECT construct. We quantitatively determined the differences in isometric twitch force and the sarcomeric proteoforms between two groups of hiPSC-ECTs that differed in the duration of time of 3D-ECT culture. Importantly, by using this integrated method we discovered a new and strong correlation between the measured contractile parameters and the phosphorylation levels of alpha-tropomyosin between the two groups of hiPSC-ECTs. The integration of functional assessments together with molecular characterization by top-down proteomics in the same hiPSC-ECT construct enables a holistic analysis of hiPSC-ECTs to accelerate their applications in disease modeling, cardiotoxicity, and drug discovery. Data are available via ProteomeXchange with identifier PXD022814.

Graphical Abstract



Keywords

human pluripotent stem cell; engineered cardiac tissue; cardiac function; top-down proteomics; proteoform

INTRODUCTION

Human induced pluripotent stem cell-derived cardiomyocytes (hiPSC-CM) are a promising model system for disease modeling, cardiotoxicity screening, and drug discovery. $^{1-4}$ Three-dimensional (3D) engineered cardiac tissue (ECT) constructs made from hiPSC-CMs are particularly appealing due to their closer representation of the structural and functional complexity of the heart compared to two-dimensional (2D) hiPSC-CM monolayers. $^{5-8}$ However, 3D hiPSC-ECT constructs have yet to completely mimic the properties of the adult heart (e.g., contractility, electrophysiology, metabolism, and isoform expression), necessitating robust metrics to characterize hiPSC-ECTs. $^{8-11}$ Traditional properties used to assess hiPSC-ECT function and molecular composition include measurement of contractile properties, cell morphology, electrophysiological properties, and β -adrenergic response among others. 8,10 Unfortunately, many of these properties are semiquantitative and the results can be influenced by confounding variables such as batch-to-batch variability and duration of time spent in culture. 8

Top-down mass spectrometry (MS)-based proteomics is a premier technology for the measurement of proteoforms—the numerous protein products originating from a single gene as a result of events such as genetic mutations, alternative splicing, and post-translational modifications (PTMs). ¹²⁻¹⁴ As an adjunct to functional assessments, top-down proteomics offers a unique opportunity to obtain an in-depth assessment of hiPSC-ECT by measuring the molecular specificity and abundance of various proteoforms. ¹¹ In a typical top-down proteomics workflow, proteins are extracted from cells or tissue and directly analyzed by high resolution liquid chromatography tandem mass spectrometry (LC-MS/MS). ¹⁵⁻²¹ By forgoing the enzymatic digestion step of the conventional bottom-up proteomics, combinatorial PTMs and protein isoforms with high sequence homology can be measured.

Both protein isoform composition and dynamic changes in PTMs are known to significantly influence cardiac performance. ^{22,23} Top-down proteomics offers a complementary and highly informative molecular analysis in the comprehensive assessment of hiPSC-ECT constructs. However, functional or molecular characterization are frequently performed on separate hiPSC-ECTs, ¹¹ which might confound results due to cellular heterogeneity, variable culture conditions, and the potential of karyotypic irregularities. ⁸ Therefore, measurement of both functional and molecular properties on the same hiPSC-ECTs would permit a direct correlation to better define cause and effect relationships.

Here we report the sequential analysis of contractile function with top-down proteomic analysis using the same hiPSC-ECT construct. Using this integrated approach, we compared twitch-force measurements and sarcomeric proteoform profiles from two groups of hiPSC-ECTs that differed in the duration of 3D-ECT culture. Specifically, we found differences in contractile performance and correlated these differences with the measured sarcomeric proteoforms between the two groups. Moreover, we identified a new and strong correlation between the measured contractile parameters and the phosphorylation levels of alphatropomyosin (*a*-Tpm) between the two groups of hiPSC-ECTs. The integration of functional measurements with top-down proteomics using the same ECT construct provides a more accurate and reliable correlation between the function and molecular composition of hiPSC-ECTs for disease modeling, cardiotoxicity and drug discovery. To the best of our knowledge, this is the first time that functional assessments and proteomics are performed within the same sample.

MATERIALS AND METHODS

Chemicals and Reagents

All reagents were purchased from Millipore Sigma (St. Louis, MO, USA) and Fisher Scientific (Fair Lawn, NJ, USA) unless noted otherwise. All solutions were prepared with HPLC grade water (Fisher Scientific, Fair Lawn, NJ, USA).

hiPSC Cell Culture

One hiPSC line, DF19–9–11T, obtained from the WiCell Research Institute, was cultured in StemFlex medium (Thermo Fisher A3349401) according to the manufacturer's protocol. In short, cryopreserved hiPSCs were thawed onto Matrigel (GFR, BD Biosciences) coated 6-well plates. hiPSCs were maintained in StemFlex media at 37 °C; 5% CO₂ until they were 70–80% confluent prior to passaging. For passaging, hiPSCs were dissociated using Versene solution (Thermo Fisher 15040066), resuspended in StemFlex media, and plated onto Matrigel (Corning) coated plates.

Differentiation of hiPSCs to Cardiomyocytes

hiPSCs from the DF19–9–11T line were differentiated to hiPSC-CMs using a small molecule-directed protocol similar to that described previously. 11,24 In short, hiPSCs maintained on the StemFlex/Matrigel system were dissociated into single cells and seeded onto Matrigel-coated 6-well plates at 1.9×10^6 cells/well in StemFlex medium. Cells were cultured for 5 days in StemFlex medium (1 day post-100% confluence, at which time

differentiation was initiated and marked Day 0). On Day 0 StemFlex medium was replaced with 2 mL/well RPMI supplemented with B27 without insulin (Gibco) and 9 μ M CHIR99021 (GSK-3 inhibitor, Tocris Bioscience). Precisely 24 h later (Day 1) medium was changed to 3 mL/well RPMI +B27 without insulin and cells were cultured in this medium for 48 h (Day 3). On Day 3, the medium was changed to 3 mL/well RPMI+B27 without insulin supplemented with 5 μ M IWP-4 (Stemgent). 48 h later (Day 5), the medium was changed to 3 mL RPMI+B27 without insulin. On Day 7, the medium was changed to RPMI +B27 complete supplement (with insulin; Gibco), and the differentiated cells were maintained in this medium until Day 15 with medium changes every 48–72 h. On Day 15, cells from wells containing ≥60% beating cells by visual inspection were dissociated with 10× TrypLE (ThermoFisher Scientific) according to the manufacturer's protocol. Following resuspension in EB20 medium, ²⁵ cells were replated on SyntheMax (Corning) coated 6-well plates. 48 h after replating, hiPSC-CMs were purified using CDM3L media (RPMI 1640 no glucose (Life Technologies), 500 µg/mL recombinant human albumin, 213 µg/mL L ascorbic acid 2-phosphate, and 4 mM L-lactic acid (Sigma-Aldrich)) for 7 days with media changes every 48–72 h.²⁶ Following selection, hiPSC-CMs were maintained in RPMI with B27 supplement (with insulin) until Day 30 at which point hiPSC-CMs were dissociated for hiPSC-ECT generation.

Differentiation of hiPSCs to Cardiac Fibroblasts

hiPSCs from the DF19-9-11T line were differentiated to cardiac fibroblasts (hiPSC-CFs) using the GiFGF protocol as previously described.²⁷ hiPSCs were dissociated with 1 mL/ well Versene solution (Gibco) at 37 °C for 5 min, seeded on Matrigel (GFR, BD Biosciences) and coated 6-well plates at the density of 1.9×10^6 cells/well in mTeSR1 medium (STEMCELL Technologies) supplemented with 10 μM ROCK inhibitor (Y-27632) (Tocris). Cells were subsequently cultured for 5 days in mTeSR1 medium with daily medium changes, and differentiation was started when the cells reached 100% confluency (Day 0). At Day 0, the medium was changed to 2.5 mL RPMI+B27 without insulin and supplemented with 12 μ M CHIR99021 (Tocris), and cells were treated in this medium for 24 h (Day 1). After Day 1, the medium was changed to 2.5 mL RPMI+B27 without insulin (Gibco) and cells were cultured in this medium for 24 h (Day 2). After Day 2 but within 24 h (before Day 3), the medium was changed to 2.5 mL of the CFBM medium²⁷ supplemented with 75 ng/mL bFGF (WiCell Research Institute). For every other day until Day 20, cells were fed with CFBM+75 ng/mL bFGF. The purity of the differentiated hiPSC-CFs were assessed by flow cytometry 20 days after differentiation. The hiPSC-CFs were passaged, expanded, and cryopreserved as previously described.²⁷

hiPSC-ECT Generation

Day 30 DF19–9–11T hiPSC-CMs were visually inspected and wells containing \geq 95% beating cells were dissociated with 10× TrypLE (ThermoFisher Scientific) following the manufacturer's protocol and counted using a hemocytometer. hiPSC-CMs were subsequently resuspended at 1–2 × 10⁶ CM/mL in fibrin ECT media (60.3% high-glucose DMEM; 20% F12 nutrient supplement; 1 mg/mL gentamicin; 8.75% FBS; 6.25% horse serum; 1% HEPES; 1× nonessential amino acid cocktail; 3 mM sodium pyruvate; 0.004% (wt/vol) NaHCO₃; 1 μ g/mL insulin; 400 μ M tranexamic acid and 17.5 μ g/mL aprotinin)¹¹

and incubated for 1 h on a rotating platform at 37 °C to form small and uniform clusters of viable hiPSC-CMs. DF19–9–11T hiPSC-CFs were dissociated using $1\times$ TrypLE (ThermoFisher Scientific) based on the manufacturer's protocol and counted with a hemocytometer. After rotational culture, 2×10^6 hiPSC-CMs were mixed with 2×10^5 hiPSC-CFs in 200 μ L fibrin ECT media per hiPSC-ECT. To this cell mixture, 1.25 mg/mL fibrinogen and 0.5 unit of thrombin were added. This cell-matrix mixture was rapidly mixed and loaded onto a 20×3 mm cylindrical mold of FlexCell TissueTrain silicone membrane culture plate, followed by incubation under preprogrammed vacuum condition for 60 min at 37 °C supplied with 5% CO₂ to allow for attachment of the hiPSC-ECT constructs to the nylon tabs at each end of the TissueTrain well. Following polymerization of the fibrin matrix, hiPSC-ECT were fed with ECT media, carefully separated from the plate surface with a sterile pipet, and cultured either 23 or 51 days with media changes every 2–3 days.

Twitch Force Measurements

Isometric twitch force was measured in hiPSC-ECT using procedures similar to those previously reported. 11,24,27,28 In brief, each hiPSC-ECT construct was transferred from the culture dish to a model 801B small intact fiber test apparatus (Aurora Scientific) in Krebs-Henseleit buffer (119 mmol/L NaCl; 4.6 mmol/L KCl; 1.2 mmol/L MgCl₂; 1.8 mmol/L CaCl₂; 12 mmol/L Glucose; 1.2 mmol/L KH₂PO₄, 25 mmol/L NaHCO₃, gassed with 95% O₂/5% CO₂ (pH 7.4)). hiPSC-ECT constructs were attached with sutures between a model 403A force transducer (Aurora Scientific) and a stationary arm and perfused with 37 °C Krebs-Henseleit buffer at a rate of 1 mL/min and field-stimulation initiated at 1 Hz (2.5 ms, 12.5 V). The longitudinal length of each construct was increased stepwise until maximal twitch force was obtained to establish the Frank-Starling relationship. Constructs were allowed to equilibrate for 20 min with constant perfusion. Following equilibration, twitch force production was measured with pacing at a frequency of 1 Hz. Twitch force data was analyzed utilizing IonWizard 6.0 software (IonOptix) by averaging data from 40 to 60 successive contractions. This data was exported to Microsoft Excel and the magnitude of force generated, in addition to the kinetics of force generation and relaxation were calculated. The data was subsequently exported to Prism GraphPad 8.0.1 for generating graphs and statistical analysis.

Sarcomeric Protein Extraction from hiPSC-ECT

The functionally assessed hiPSC-ECTs were washed with 1.0 mL of Mg²⁺/Ca²⁺-free DPBS then centrifuged for 5 min at 1100g, 4 °C (Sorvall Legend Micro 21R; Thermo Fisher Scientific, Am Kalkberg, Germany). The supernatant was discarded to remove residual cell culture media components. The hiPSC-ECT samples were homogenized in 50 μ L of HEPES extraction buffer (25 mM HEPES (pH 7.4), 60 mM NaF, 1 mM L-methionine, 1 mM DTT, 1 mM PMSF in isopropanol, 1 mM Na₃VO₄ containing protease and phosphatase inhibitors) by a Teflon pestle (1.5 mL microcentrifuge tube, flat tip; Thomas Scientific, Swedesboro, NJ, USA) at 4 °C. The homogenate was centrifuged for 30 min at 21 000g, 4 °C and the supernatant comprising mostly cytosolic proteins was collected, labeled (HEPES1), and kept at -80 °C. The pellet was then resuspended in an additional 50 μ L of HEPES extraction buffer to further remove any remaining cytosolic proteins. The homogenate was centrifuged for 30 min at 21 000g, 4 °C and the supernatant was collected, labeled (HEPES2), and stored

at -80 °C. The sarcomere enriched protein pellets were frozen at -80 °C until both groups of hiPSC-ECTs were ready to be analyzed via LC-MS/MS to reduce instrumental variation. The sarcomere enriched protein pellets were then thawed and homogenized in 40 μ L of TFA extraction buffer (1% TFA, 5 mM TCEP, 5 mM L-methionine) at 4 °C using a Teflon pestle. The homogenate was centrifuged for 30 min at 21 000g, 4 °C and the resulting supernatant was collected and labeled as TFA extract. Subsequently, the TFA extract was desalted with five volumes of mobile phase A (MPA; 0.1% formic acid in HPLC grade water) utilizing a 10 kDa molecular weight cutoff filter (Amicon; Merck KGaA, Darmstadt, Germany). A protein assay (Cat. #5000006; BioRad, Hercules, CA, USA) was performed using bovine serum albumin for the linear curve to determine the total protein concentration of the sarcomere protein extract for normalization prior to top-down proteomics analysis.

Reverse Phase Chromatography and Top-Down MS Analysis

Reverse phase chromatography (RPC) was performed using a NanoAcquity ultrahigh pressure LC system (Waters, Milford, MA, USA). 500 ng of the TFA protein extracts were loaded on a home-packed PLRP-S capillary column (200 mm long, 0.25 mm i.d., 5 μ m particle size, 1000 Å pore size; Agilent Technology, Santa Clara, CA, USA). Mobile phase B (MPB) contained 0.1% formic acid in 50:50 acetonitrile and ethanol. The column was maintained at 60 °C with a constant 8 µL/min flow rate. The RPC gradient consisted of the following concentrations of MPB: 10% MPB at 0 min, held at 10% until 5 min, 65% at 65 min, 95% at 70 min, held at 95% until 75 min, adjusted back to 10% at 75.1 min, and held at 10% until 80 min. The eluted proteins were electrosprayed into a Bruker Impact II quadrupole-time-of-flight (Q-TOF) mass spectrometer (Bruker Daltonics, Bremen, Germany). End plate offset and capillary voltage were set at 500 and 4500 V, respectively. The nebulizer was set to 0.3 bar, and the dry gas flow rate was 4.0 L/min at 200 °C. The quadrupole low mass was set to 650 m/z. A scan rate of 1 Hz over the 200–3000 m/z range was used to collect mass spectra. Three technical replicates were collected for one sample from each hiPSC-ECT group to ensure instrument reproducibility and stability. Datadependent online MS/MS analysis was performed by selecting the top 3 most abundant ions, followed by fragmentation via collisionally activated dissociation (CAD) with the collisional energy between 15 and 30 eV. A scan rate of 2-4 Hz across 200-3000 m/z mass range was used to collect MS/MS spectra. Active exclusion was activated after 4 MS/MS spectra and the selected ions were excluded for 2 min. The intact masses of the precursor ions were determined based on the first LC-MS run, and the fragment ions were determined by the following LC-MS/MS run.

Data Analysis

OtofControl 3.4 (Bruker Daltonics) was used to collect all LC-MS/MS data. DataAnalysis 4.3 software (Bruker Daltonics) was used to process and analyze the MS data. A smoothing width of 2.01 s using the Gauss algorithm was implemented for all the chromatograms. The Maximum Entropy algorithm within the DataAnalysis 4.3 software was used to deconvolute sarcomeric proteins of interest. For proteins that were isotopically resolved, the resolving power for the Maximum Entropy deconvolution was set to 50 000. The sophisticated numerical annotation procedure (SNAP) algorithm was applied to determine the monoisotopic masses of all observed ions. The top three most abundant charge state ions of

the sarcomeric proteins of interest were used to produce extracted ion chromatograms (EICs). Relative abundance of the selected protein isoforms was measured by the ratio of their area under the curve (AUC) from their respective EICs (eq 1).¹¹

Protein Isoform Ratio =
$$\frac{AUC \text{ from EIC of Isoform 1}}{AUC \text{ form EIC of Isoform 2}}$$
(1)

Relative quantification of protein phosphorylation was calculated by deconvoluting mass spectra of interest using the Maximum Entropy algorithm, and the relative abundance of a particular proteoform (P_{total}) is reported as the ratio of the peak intensity of the proteoform (mol P_{i}) to the summed peak intensities of all proteoforms (mol protein) of the same protein (eq 2).¹¹

$$P_{\text{total}} = \frac{\text{mol } P_{\text{i}}}{\text{mol protein}} \tag{2}$$

Tandem mass spectra of sarcomeric proteoforms identified by intact mass were exported from DataAnalysis 4.3 software as .ascii files and processed with MASH Explorer²⁹ equipped with the MS-align+³⁰ algorithm to manually validate ions and confirm protein identification. In the tandem mass spectra, the fragment ions were assigned based on the protein sequence of myofilament protein isoforms in the UniProt-SwissProt human database. Allowance was made for possible PTMs, such as N-terminal acetylation and trimethylation. Monoisotopic masses were used for all proteoform determinations and a mass tolerance of 10 ppm was implemented for all fragment ion validation.

Statistical Analysis

Statistical analysis of twitch force amplitude, time from pacing stimulus to twitch force peak (CT₁₀₀), time from twitch force peak to 50% twitch force decay (RT₅₀), and time from 50% to 90% twitch force decay (RT₅₀₋₉₀), relative phosphorylation, and isoform ratios between the different groups of hiPSC-ECTs were determined by a Student's two-tailed t test assuming equal variances. ns indicated a p > 0.05, * indicated a p < 0.05, and ** indicated a p < 0.01 by Student's two-tailed t test with equal variances. Standard error of the mean was used for calculating the variation between the two groups of hiPSC-ECTs. Phosphorylation and contractile parameter values were fit to a multivariate linear model with age as the independent variable. After model fitting, the normalized contractile parameter and phosphorylation values were obtained using the model's residuals and the estimated respective age coefficients.

RESULTS AND DISCUSSION

Functional Assessment of hiPSC-ECTs

The objective of this study was to develop a robust method to measure the contractile properties of hiPSC-ECTs together with sarcomeric proteoform composition by integrating isometric twitch force measurements and top-down proteomics in the same hiPSC-ECT (Figure 1). In this case, we chose to study two groups of hiPSC-ECTs which spent 23 and 51

days in 3D-ECT culture respectively (Supplementary Figure S1). Lactate purified hiPSC-CMs and low passage isogenic hiPSC-CFs were used in a 10:1 ratio in hiPSC-ECT constructs (Supplementary Figure S1).^{27,31} Cells were mixed with fibrinogen and thrombin and seeded into molds to form hiPSC-ECTs. The hiPSC-ECTs of the same batch were then cultured and randomly selected at Day 23 and Day 51 for sequential functional assessments followed by top-down proteomic characterization. Of note, hiPSC-ECTs with the same genetic background were generated with hiPSC-CMs and hiPSC-CFs from the same differentiation batch to minimize confounding factors such as differentiation efficiency, batch effects, and feeding schedule among other factors.

We measured the contractile properties of the Day 23 and Day 51 hiPSC-ECTs at the time of harvest (Figure 1). hiPSC-ECT constructs were mounted to a force transducer in a physiologic chamber and stretched to optimal sarcomere length with electrical pacing at 1 Hz at 37 °C. Following equilibration, we assessed twitch force amplitude, time from pacing stimulus to twitch force peak (CT₁₀₀), time from twitch force peak to 50% twitch force decay (RT₅₀), and time from 50% to 90% twitch force decay (RT₅₀–90) (Figure 2). Interestingly, the Day 51 hiPSC-ECTs yielded a statistically significant increase in twitch force amplitude, reduced CT₁₀₀ and RT₅₀ intervals, and a prolonged RT₅₀–90 interval compared to the Day 23 hiPSC-ECTs. Collectively, the contractile measurements indicate that the Day 51 hiPSC-ECTs display more mature contractile properties compared to the Day 23 hiPSC-ECTs.

Top-Down Proteomics of hiPSC-ECTs

After the measurement of the functional properties, we then sequentially assessed the hiPSC-ECT sarcomeric proteoform profiles arising from the same hiPSC-ECT using top-down proteomics (Figure 1). Immediately following hiPSC-ECT mechanical property measurements, sarcomeric proteins were extracted for top-down proteomics using the same hiPSC-ECT construct. A dual lysis buffer containing HEPES (pH = 7) was used to deplete highly abundant cytosolic proteins, leaving a sarcomere-enriched pellet, which were frozen (-80 °C) until both groups of hiPSC-ECTs were ready to be analyzed by LC-MS/MS (Supplementary Figure S1). Sarcomeric proteins were extracted from the pellets using a MS-compatible, trifluoroacetic acid (TFA) buffer (pH = 2) and equal amounts of proteins were analyzed by LC-MS/MS. Aliquots of every sample were saved for SDS-PAGE to visualize the extracted proteins and confirm the reproducibility of the extraction methods (Supplementary Figure S2). Our method is highly reproducible, demonstrated by highly consistent retention time and spectral intensity of three LC-MS/MS technical replicates of a Day 23 and 51 hiPSC-ECT (Supplementary Figure S3, Supplementary Figure S4).

Major sarcomeric proteins, such as slow skeletal troponin I (ssTnI, gene: *TNNII*), isoform 6 of cardiac troponin T (cTnT6, gene: *TNNT2*), cardiac troponin I (cTnI, gene: *TNNI3*), *a*-Tpm (gene: *TPMI*), the ventricular isoform of myosin light chain 1 (MLC-1v, gene: *MYL3*), the atrial isoform of myosin light chain 1 (MLC-1a, gene: *MYL4*), the ventricular isoform of myosin light chain 2 (MLC-2v, gene: *MYL2*), the atrial isoform of myosin light chain 2 (MLC-2a, gene: *MYL7*), alpha actin (*a*-actin, gene: *ACTCI*), and troponin C (TnC, gene: *TNNCI*), were measured in the hiPSC-ECTs (Figure 3A, Supplementary Figure S4). The

abundance of each sarcomeric protein is represented by the AUC of their corresponding EICs and this AUC value was used to compare the protein isoform abundances for all samples. The base peak chromatogram (BPC), a trace of the most abundant ion eluting from the LC column as a function of time, revealed the major sarcomeric proteins found in the hiPSC-ECTs (Supplementary Figure S5). Importantly, the reproducible LC-MS/MS results for the various sarcomeric proteins enabled the reliable relative quantification of specific proteoforms between the Day 23 and Day 51 hiPSC-ECT groups.

One of the unique benefits of this new integrated method is the ability to use LC to separate sarcomeric proteins with high sequence homology, such as MLC-1v and MLC-1a, and confirm their identification via MS/MS (Figure 3A, Supplementary Figure S6) without requiring separate hiPSC-ECT constructs. Online CAD was employed to fragment sarcomeric protein precursor ions (Supplementary Figure S6A), which generates *b* and *y* ions for protein sequence characterization (Supplementary Figure S6B). These CAD ions were used to confidently identify the MLC isoforms despite them sharing high sequence homology. The protein sequence fragmentation map, generated from the online LC-MS/MS method of MLC-1v and MLC-1a, shows all ions used for protein identification (Supplementary Figure S6C). In addition, N-terminal methionine truncations as well as various PTMs such as trimethylation and acetylation were detected on MLC-1v and MLC-1a, respectively.³² Our results indicated that there was not a statistically significant change in the ratio of MLC-1v to MLC-1a between the two groups of hiPSC-ECTs (Supplementary Figure S7).

Several sarcomeric PTMs and isoforms were observed in the hiPSC-ECTs as seen in the deconvoluted mass spectra (Figure 3B, Supplementary Figure S8, Supplementary Figure S9). Unphosphorylated and phosphorylated cTnI were detected in both Day 23 and Day 51 hiPSC-ECTs; nevertheless, the relative phosphorylation levels between the groups was not statistically significant (Figure 3, Supplementary Figure S10). cTnI is part of the troponin complex on the thin filament of the sarcomere and phosphorylation of cTnI shifts calcium sensitivity to the right and plays a role in the facilitation of more rapid relaxation. ^{21,33} Notably, cTnI proteoforms were detected in the Day 23 hiPSC-ECTs, whereas in our previous work¹¹ no cTnI was observed in the earlier stage hiPSC-ECTs. cTnI is the major isoform of the troponin complex observed in adult heart tissue, whereas ssTnI is predominantly expressed in fetal cardiac tissue. This finding suggests that the addition of hiPSC-CFs in the hiPSC-ECT constructs may accelerate tissue maturation, as hiPSC-CFs were not used in the previous study. 11 Although cTnI was detected in both groups, the relative ratio of cTnI to ssTnI significantly increased from Day 23 to Day 51 hiPSC-ECTs (Supplementary Figure S10). This trend may reflect progressive maturation due to the differences in the amount of time spent in culture between the two groups. Whereas each sample contained phosphorylated cTnI, there were variations in the relative phosphorylation from sample to sample (Supplementary Figure S9A) within and between the two hiPSC-ECTs groups. The observed sample heterogeneity underscores the importance of developing methods that integrate multiple assessments on the same hiPSC-ECT construct to support reliable correlations and accurate conclusions.

In particular, α -Tpm is another thin filament protein involved in contractility and is the major Tpm isoform found in the human heart.³⁴ Unphosphorylated and phosphorylated α -Tpm was detected in Day 23 and Day 51 hiPSC-ECTs (Figure 3B, Supplementary Figure S9B). For the Day 51 hiPSC-ECTs, the phosphorylated α -Tpm proteoform was significantly decreased compared to the Day 23 hiPSC-ECTs, a trend previously observed with increased time in culture.¹¹

cTnT6 regulates the Ca²⁺-mediated interaction between myosin thick filaments and actin thin filaments during cardiac contraction and relaxation.³³ Our data reveals that the predominant form of cTnT6 was found to be the phosphorylated proteoform (Figure 3B, Supplementary Figure S9C). We report the first top-down proteomics analysis showing a significant decrease in the relative abundance of phosphorylated cTnT6 between the Day 23 and Day 51 hiPSC-ECTs a trend previously observed in (2D) hiPSC-CM monolayers.¹¹

Integration of Functional Assessments and Top-Down Proteomics Data

Using the acquired functional and top-down proteomic data from the same hiPSC-ECT, we next sought to integrate the metrics to identify trends between the two groups. We plotted the relative phosphorylation levels of α -Tpm, cTnT6, and cTnI as a function of twitch force magnitude, CT₁₀₀, and RT₅₀ to determine if there were any observed trends in contractile performance that might be due to causative effects of the measured molecular variables (Figure 4, Supplementary Figure S11, and Supplementary Figure S12). Interestingly, we found decreased levels of a-Tpm phosphorylation to be significantly associated with increased twitch force production and accelerated rates of contraction and relaxation (Figure 4A-C). Strikingly, we found that there was an extremely high correlation ($R^2 = 0.9666$) between the CT_{100} and the phosphorylation levels of α -Tpm between the two groups of hiPSC-ECTs (Figure 4A). As increased twitch force production and accelerated rates of contraction and relaxation are also associated with maturation of the human myocardium³⁵ and prolonged culture of hiPSCs-ECT due to maturation of the Ca²⁺-handling system and expression of more mature sarcomeric protein isoforms, 11 we also show that twitch force magnitude and RT₅₀ show a significant association, $R^2 = 0.7844$ and $R^2 = 0.7829$, respectively, with a-Tpm phosphorylation (Figure 4B,C). However, when we performed multivariate statistics to account for the effects of time spent in culture, these associations where much more poorly correlated (Supplementary Figure S12B,C), whereas the correlation of a-Tpm phosphorylation with CT_{100} remained strong ($R^2 = 0.8216$) (Supplementary Figure S12A). This analysis suggests a cumulative effect of time in hiPSC-ECT culture and decreased a-Tpm phosphorylation on contractile performance, particularly CT_{100} .

Phosphorylation of α -Tpm is known to be strongly associated with cardiac maturation, decreasing from \sim 60–70% in fetuses and newborns to \sim 30% in adults. ^{11,36} Though the physiological impact of α -Tpm phosphorylation on cardiac function is not fully understood, ³⁷ several studies in transgenic mouse models found that either increasing or decreasing phosphorylation of α -Tpm can yield hypertrophic or dilated cardiomyopathy phenotypes without altering calcium-sensitivity or crossbridge cooperativity. ^{36,37} Consistent with our data in hiPSC-ECTs, transgenic overexpression of a phosphomimetic α -Tpm in mice

trended toward slower contractile kinetics and significantly accelerated relaxation.³⁷ While cTnT6 phosphorylation levels were correlated with contractile performance (Supplementary Figure S11A-C), this association was not as strongly correlated compared to the relationship between α -Tpm phosphorylation. When taking a multivariate statistics approach, to account for the codependence effect of time spent in culture, these associations largely disappeared (Supplementary Figure S12D-F). In addition, the cTnI phosphorylation levels were poorly correlated with contractile performance both before and after accounting for time spent in culture (Supplementary Figure S11D-F, Supplementary Figure S12G-I).

In summary, we report for the first time an integrated method that permits sequential functional assessments and top-down proteomics analysis on the same hiPSC-ECT construct. Taken together, top-down proteomics of sarcomeric proteoforms provides an important molecular assessment of hiPSC-ECTs. Moreover, the direct integration of functional assessments with top-down proteomics using the same ECT construct provides accurate correction between molecular composition and function. Our results indicate that the contractile properties and sarcomeric proteoforms between the two groups of hiPSC-ECTs were distinctly changed and that the underlying heterogeneity of hiPSC-ECTs can be analyzed by this integrated approach. Importantly, we found that there were noticeable heterogeneity in the sarcomeric proteoforms and functional measurements, such as cTnI phosphorylation and twitch force magnitude, within the specific groups emphasizing the benefit of multiple assessments on the same hiPSC-ECT construct. Furthermore, the unique value of this integrated approach is illustrated by our discovery that there is a distinct correlation between the speed of cardiac contractility as measured by the functional properties and the phosphorylation levels of α -Tpm. Importantly, this is the first time that both functional assessments and proteomics are measured within the same sample. We acknowledge that all hiPSC-ECTs used in the current study share a common genetic background and that future studies will benefit from using multiple hiPSC lines to determine the differences in functional and proteomics properties across multiple cell lines. We anticipate that this method will prove to be cost-effective by reducing the need to culture additional hiPSC-ECTs for separate functional and proteomics measurements. We envision that this integrated method will enable the direct assessment of proteoform-level molecular details and functional attributes across various patient-derived ECT constructs to provide mechanistic support for disease modeling, drug screenings, and cell-based therapies.

Supplementary Material

Refer to Web version on PubMed Central for supplementary material.

ACKNOWLEDGMENTS

Financial support was provided by National Institutes of Health (NIH) R01 HL096971 (to Y.G.). Y.G. would also like to acknowledge R01 GM117058, GM125085, HL109810, and S10 OD018475. J.A.M. would like to acknowledge support from the Training Program in Translational Cardiovascular Science, T32 HL007936-20. T.J.K. would like to acknowledge the National Science Foundation for Grant No. EEC-1648035, NIH grants R01 HL129798 and U01 HL134764. J.C.R. would like to acknowledge financial support provided by the Wisconsin Partnership Program. We would like to thank Dr. Yanlong Zhu for his help with the instrument.

ABBREVIATIONS

3D 3-dimensional

ECT engineered cardiac tissue

hiPSC-CM human induced pluripotent stem cell-derived

cardiomyocyte

2D 2-dimensional

MS mass spectrometry

PTMs post-translational modifications

LC-MS/MS liquid chromatography tandem mass spectrometry

a-Tpm alpha tropomyosin

hiPSC-CF human induced pluripotent stem cell-derived cardiac

fibroblast

RPC reverse phase chromatography

Q-TOF quadrupole-time-of-flight

CAD collision-activated dissociation

SNAP sophisticated numerical annotation procedure

AUC area under the curve

EIC extracted ion chromatogram

 P_{total} relative abundance of a particular proteoform

 $mol P_i$ peak intensity of the proteoform

mol protein summed peak intensities of all proteoforms

S/N signal-to-noise

CT₁₀₀ time from pacing stimulus to twitch force peak

RT₅₀ time from twitch force peak to 50% twitch force decay

RT₅₀₋₉₀ time from 50% to 90% twitch force decay

ssTnI slow skeletal troponin I

cTnT6 isoform 6 of cardiac troponin T

cTnI cardiac troponin I

MLC-1v ventricular isoform of myosin light chain 1

MLC-1a atrial isoform of myosin light chain 1

MLC-2v ventricular isoform of myosin light chain 2

MLC-2a atrial isoform of myosin light chain 2

a-actin alpha actin

TnC troponin C

BPC base peak chromatogram

REFERENCES

- (1). Lian X; Zhang J; Azarin SM; Zhu K; Hazeltine LB; Bao X; Hsiao C; Kamp TJ; Palecek SP Directed Cardiomyocyte Differentiation from Human Pluripotent Stem Cells by Modulating Wnt/β-Catenin Signaling under Fully Defined Conditions. Nat. Protoc 2013, 8 (1), 162–175. [PubMed: 23257984]
- (2). Burridge PW; Keller G; Gold JD; Wu JC Production of de Novo Cardiomyocytes: Human Pluripotent Stem Cell Differentiation and Direct Reprogramming. Cell Stem Cell. 2012, 10 (1), 16–28. [PubMed: 22226352]
- (3). Karakikes I; Ameen M; Termglinchan V; Wu JC Human Induced Pluripotent Stem Cell-Derived Cardiomyocytes: Insights into Molecular, Cellular, and Functional Phenotypes. Circ. Res 2015, 117 (1), 80–88. [PubMed: 26089365]
- (4). Zhang J; Klos M; Wilson GF; Herman AM; Lian X; Raval KK; Barron MR; Hou L; Soerens AG; Yu J; Palacek SP; Lyons GE; Thomson JA; Herron TJ; Jalife J; Kamp TJ Extracellular Matrix Promotes Highly Efficient Cardiac Differentiation of Human Pluripotent Stem Cells: The Matrix Sandwich Method. Circ. Res 2012, 111 (9), 1125–1136. [PubMed: 22912385]
- (5). Feric NT; Radisic M Maturing Human Pluripotent Stem Cell-Derived Cardiomyocytes in Human Engineered Cardiac Tissues. Adv. Drug Delivery Rev 2016, 96 (1), 110–134.
- (6). Ralphe JC; De Lange WJ 3D Engineered Cardiac Tissue Models of Human Heart Disease: Learning More from Our Mice. Trends Cardiovasc. Med 2013, 23 (2), 27–32. [PubMed: 23295081]
- (7). Jackman CP; Shadrin IY; Carlson AL; Bursac N Human Cardiac Tissue Engineering: From Pluripotent Stem Cells to Heart Repair. Curr. Opin. Chem. Eng 2015, 7 (1), 57–64. [PubMed: 25599018]
- (8). Weinberger F; Mannhardt I; Eschenhagen T Engineering Cardiac Muscle Tissue. Circ. Res 2017, 120 (9), 1487–1500. [PubMed: 28450366]
- (9). Borovjagin AV; Ogle BM; Berry JL; Zhang J From Microscale Devices to 3D Printing: Advances in Fabrication of 3D Cardiovascular Tissues. Circ. Res 2017, 120 (1), 150–165. [PubMed: 28057791]
- (10). Veldhuizen J; Migrino RQ; Nikkhah M Three-Dimensional Microengineered Models of Human Cardiac Diseases. J. Biol. Eng 2019, 13 (1), 29. [PubMed: 30988697]
- (11). Cai W; Zhang J; de Lange WJ; Gregorich ZR; Karp H; Farrell ET; Mitchell SD; Tucholski T; Lin Z; Biermann M; McIlwain SJ; Ralphe JC; Kamp TJ; Ge Y An Unbiased Proteomics Method to Assess the Maturation of Human Pluripotent Stem Cell-Derived Cardiomyocytes. Circ. Res 2019, 125 (11), 936–953. [PubMed: 31573406]
- (12). Chen B; Brown KA; Lin Z; Ge Y Top-Down Proteomics: Ready for Prime Time? Anal. Chem 2018, 90, 110–127. [PubMed: 29161012]
- (13). Smith LM; Kelleher NL; Linial M; Goodlett D; Langridge-Smith P; Goo YA; Safford G; Bonilla L; Kruppa G; Zubarev R; Rontree J Proteoform: a single term describing protein complexity. Nat. Methods 2013, 10, 186. [PubMed: 23443629]
- (14). Smith LM; Kelleher NL Proteoforms as the next proteomics currency. Science 2018, 359, 1106. [PubMed: 29590032]

(15). Wei L; Gregorich ZR; Lin Z; Cai W; Jin Y; McKiernan SH; McIlwain S; Aiken JM; Moss RL; Diffee GM; Ge Y Novel Sarcopenia-Related Alterations in Sarcomeric Protein Post-Translational Modifications (PTMs) in Skeletal Muscles Identified by Top-down Proteomics. Mol. Cell. Proteomics 2018, 17 (1), 134–145. [PubMed: 29046390]

- (16). Lin Z; Wei L; Cai W; Zhu Y; Tucholski T; Mitchell SD; Guo W; Ford SP; Diffee GM; Ge Y Simultaneous Quantification of Protein Expression and Modifications by Top-down Targeted Proteomics: A Case of the Sarcomeric Subproteome. Mol. Cell. Proteomics 2019, 18 (3), 594–605
- (17). Ntai I; Fornelli L; DeHart CJ; Hutton JE; Doubleday PF; LeDuc RD; van Nispen AJ; Fellers RT; Whiteley G; Boja ES; Rodriguez H; Kelleher NL Precise Characterization of KRAS4b Proteoforms in Human Colorectal Cells and Tumors Reveals Mutation/Modification Cross-Talk. Proc. Natl. Acad. Sci. U. S. A 2018, 115 (16), 4140–4145. [PubMed: 29610327]
- (18). Tran JC; Zamdborg L; Ahlf DR; Lee JE; Catherman AD; Durbin KR; Tipton JD; Vellaichamy A; Kellie JF; Li M; Wu C; Sweet SMM; Early BP; Siuti N; LeDuc RD; Compton PD; Thomas PM; Kelleher NL Mapping Intact Protein Isoforms in Discovery Mode Using Top-down Proteomics. Nature 2011, 480 (7376), 254–258. [PubMed: 22037311]
- (19). Tucholski T; Cai W; Gregorich ZR; Bayne EF; Mitchell SD; McIlwain SJ; de Lange WJ; Wrobbel M; Karp H; Hite Z; Vikhorev PG; Marston SB; Lal S; Li A; Dos Remedios C; Kohmoto T; Hermsen J; Ralphe JC; Jamp TJ; Moss RL; Ge Y Distinct Hypertrophic Cardiomyopathy Genotypes Result in Convergent Sarcomeric Proteoform Profiles Revealed by Top-down Proteomics. Proc. Natl. Acad. Sci. U. S. A 2020, 117 (40), 24691. [PubMed: 32968017]
- (20). Melby JA; Jin Y; Lin Z; Tucholski T; Wu Z; Gregorich ZR; Diffee GM; Ge Y Top-Down Proteomics Reveals Myofilament Proteoform Heterogeneity among Various Rat Skeletal Muscle Tissues. J. Proteome Res 2020, 19 (1), 446–454. [PubMed: 31647247]
- (21). Tiambeng TN; Roberts DS; Brown KA; Zhu Y; Chen B; Wu Z; Mitchell SD; Guardado-Alvarez TM; Jin S; Ge Y Nanoproteomics Enables Proteoform-Resolved Analysis of Low-Abundance Proteins in Human Serum. Nat. Commun 2020, 11 (1), 1–12. [PubMed: 31911652]
- (22). Fert-Bober J; Murray CI; Parker SJ; Van Eyk JE Precision Profiling of the Cardiovascular Post-Translationally Modified Proteome Where There Is a Will, There Is a Way. Circ. Res 2018, 122 (9), 1221–1237. [PubMed: 29700069]
- (23). Cai W; Tucholski TM; Gregorich ZR; Ge Y Top-down Proteomics: Technology Advancements and Applications to Heart Diseases. Expert Rev. Proteomics 2016, 13, 717–730. [PubMed: 27448560]
- (24). De Lange WJ; Hegge LF; Grimes AC; Tong CW; Brost TM; Moss RL; Ralphe JC Neonatal Mouse-Derived Engineered Cardiac Tissue: A Novel Model System for Studying Genetic Heart Disease. Circ. Res 2011, 109 (1), 8–16. [PubMed: 21566213]
- (25). Lian X; Hsiao C; Wilson G; Zhu K; Hazeltine LB; Azarin SM; Raval KK; Zhang J; Kamp TJ; Palecek SP Robust Cardiomyocyte Differentiation from Human Pluripotent Stem Cells via Temporal Modulation of Canonical Wnt Signaling. Proc. Natl. Acad. Sci U. S. A 2012, 109 (27), E1848–E1857. [PubMed: 22645348]
- (26). Burridge PW; Li YF; Matsa E; Wu H; Ong SG; Sharma A; Holmström A; Chang AC; Coronado MJ; Ebert AD; Knowles JW; Telli ML; Witteles RM; Blai HM; Bernstein D; Altman RB; Wu J Human Induced Pluripotent Stem Cell-Derived Cardiomyocytes Recapitulate the Predilection of Breast Cancer Patients to Doxorubicin-Induced Cardiotoxicity. Nat. Med 2016, 22 (5), 547–556. [PubMed: 27089514]
- (27). Zhang J; Tao R; Campbell KF; Carvalho JL; Ruiz EC; Kim GC; Schmuck EG; Raval AN; Monteiro Da Rocha A; Herron TJ; Jalife J; Thomson JA; Kamp TJ Functional Cardiac Fibroblasts Derived from Human Pluripotent Stem Cells via Second Heart Field Progenitors. Nat. Commun 2019, 10 (1), 2238. [PubMed: 31110246]
- (28). Smelter DF; de Lange WJ; Cai W; Ge Y; Ralphe JC The HCM-Linked W792R Mutation in Cardiac Myosin-Binding Protein C Reduces C6 FnIII Domain Stability. Am. J. Physiol. Hear. Circ. Physiol 2018, 314 (6), H1179–H1191.
- (29). Wu Z; Roberts DS; Melby JA; Wenger K; Wetzel M; Gu Y; Ramanathan SG; Bayne EF; Liu X; Sun R; Ong IM; McIlwain SJ; Ge Y MASH Explorer: A Universal Software Environment for Top-Down Proteomics. J. Proteome Res 2020, 19, 3867. [PubMed: 32786689]

(30). Liu X; Sirotkin Y; Shen Y; Anderson G; Tsai YS; Ting YS; Goodlett DR; Smith RD; Bafna V; Pevzner PA Protein Identification Using Top-Down. Mol. Cell. Proteomics 2012, 11 (6), M111.008524.

- (31). Tohyama S; Hattori F; Sano M; Hishiki T; Nagahata Y; Matsuura T; Hashimoto H; Suzuki T; Yamashita H; Satoh Y; Egashira T; Seki T; Muraoka N; Yamakawa H; Ohgino Y; Tanaka T; Yoichi M; Yuasa S; Murata M; Suematsu M; Fukuda K Distinct Metabolic Flow Enables Large-Scale Purification of Mouse and Human Pluripotent Stem Cell-Derived Cardiomyocytes. Cell Stem Cell 2013, 12 (1), 127–137. [PubMed: 23168164]
- (32). Gregorich ZR; Cai W; Lin Z; Chen AJ; Peng Y; Kohmoto T; Ge Y Distinct Sequences and Post-Translational Modifications in Cardiac Atrial and Ventricular Myosin Light Chains Revealed by Top-down Mass Spectrometry. J. Mol. Cell. Cardiol 2017, 107, 13–21. [PubMed: 28427997]
- (33). Tiambeng TN; Tucholski T; Wu Z; Zhu Y; Mitchell SD; Roberts DS; Jin Y; Ge Y Analysis of Cardiac Troponin Proteoforms by Top-down Mass Spectrometry. Methods Enzymol. 2019, 626 (1), 347–374. [PubMed: 31606082]
- (34). Peng Y; Yu D; Gregorich Z; Chen X; Beyer AM; Gutterman DD; Ge Y In-Depth Proteomic Analysis of Human Tropomyosin by Top-down Mass Spectrometry. J. Muscle Res. Cell Motil 2013, 34 (3–4), 199–210. [PubMed: 23881156]
- (35). Wiegerinck RF; Cojoc A; Zeidenweber CM; Ding G; Shen M; Joyner RW; Fernandez JD; Kanter KR; Kirshbom PM; Kogon BE; Wagner MB Force Frequency Relationship of the Human Ventricle Increases during Early Postnatal Development. Pediatr. Res 2009, 65 (4), 414–419. [PubMed: 19127223]
- (36). Schulz EM; Correll RN; Sheikh HN; Lofrano-Alves MS; Engel PL; Newman G; Schultz JEJ; Molkentin JD; Wolska BM; Solaro RJ; Wieczorek DF Tropomyosin Dephosphorylation Results in Compensated Cardiac Hypertrophy. J. Biol. Chem 2012, 287 (53), 44478–44489. [PubMed: 23148217]
- (37). Rajan S; Jagatheesan G; Petrashevskaya N; Biesiadecki BJ; Warren CM; Riddle T; Liggett S; Wolska BM; Solaro RJ; Wieczorek DF Tropomyosin Pseudo-Phosphorylation Results in Dilated Cardiomyopathy. J. Biol. Chem 2019, 294 (8), 2913–2923. [PubMed: 30567734]

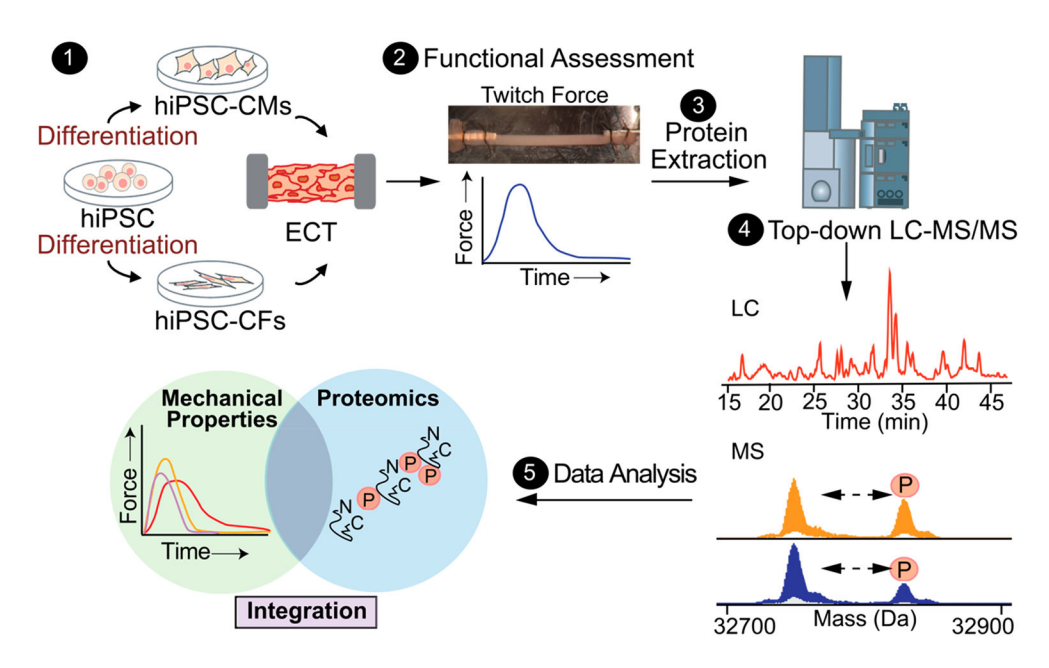


Figure 1. Schematic of integrated functional assessments and top-down proteomics workflow for the same hiPSC-ECT. (1) hiPSC are differentiated into CMs and CFs which are used to generate hiPSC-ECTs. (2) Functional assessments are performed on the hiPSC-ECTs to measure the isometric twitch force. (3) Sarcomeric proteins are extracted via a dual extraction method from the functionally tested hiPSC-ECTs. (4) Top-down proteomics is performed on the functionally tested hiPSC-ECTs. (5) The resulting data on isometric twitch force and sarcomeric proteoform quantitation of the same hiPSC-ECTs are analyzed to provide an integrated assessment of hiPSC-ECT constructs.

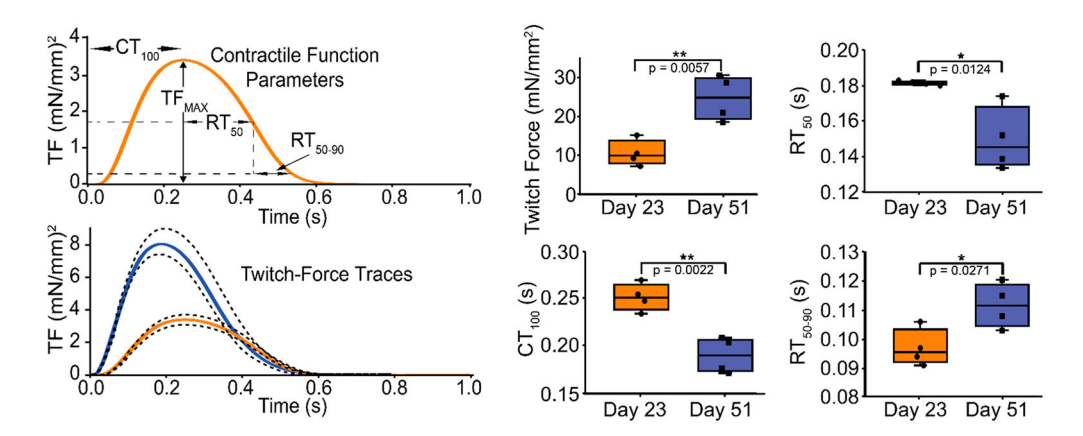


Figure 2. Contractile function in Day 23 and Day 51 hiPSC-ECTs. The trace in the top left-hand panel defines the parameters quantified in the four box-and-whisker plots below for the Day 23 (orange) and Day 51 (blue) hiPSC-ECTs. TF, twitch force magnitude (mN/mm²); CT₁₀₀, time from pacing stimulus to twitch force peak; RT₅₀, time from twitch force peak to 50% twitch force decay; RT₅₀₋₉₀, time from 50% to 90% twitch force decay. The averaged traces of the twitch force measurement of the four samples in Day 23 and Day 51 hiPSC-ECTs in the top right panel are plotted as a function of time with the standard error of the mean (SEM) shown in dashed lines. Contractile data was collected from hiPSC-ECT paced at 1 Hz at 37 °C. * refers to a p< 0.05, and ** refers to a p< 0.01 by a student's t test with equal variances.

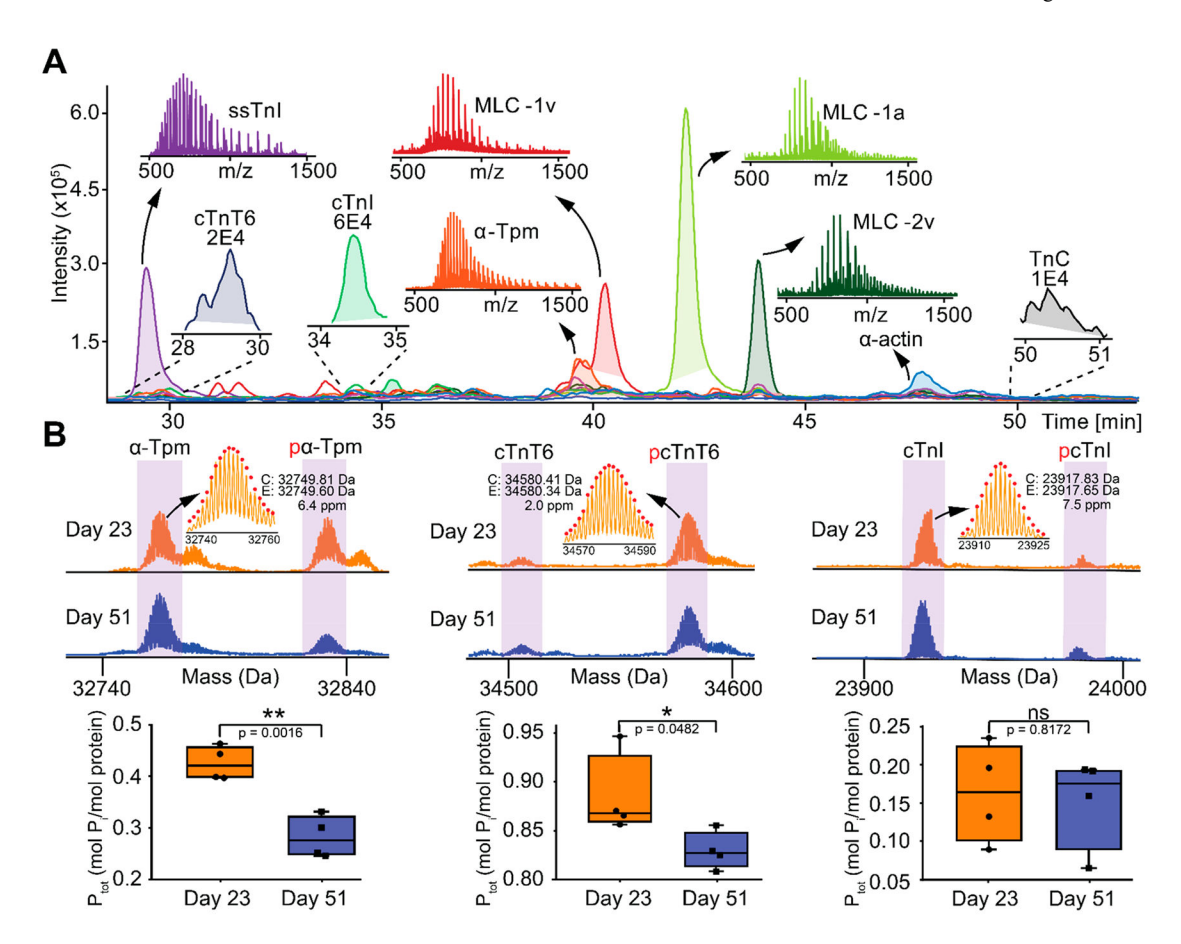


Figure 3. Top-down proteomics data of Day 23 and Day 51 hiPSC-ECTs. (A) Extracted ion chromatograms (EICs) of sarcomeric proteins in a representative Day 51 hiPSC-ECT using the top three most abundant charge state ions. The abundance of each protein is represented by the area under curve (AUC) of the corresponding EIC. Representative MS of specific proteins are shown for the major EIC peaks. (B, top) Deconvoluted mass spectra of sarcomeric proteoforms from a representative Day 23 and Day 51 hiPSC-ECT: alpha tropomyosin (α -Tpm), cardiac troponin T isoform 6 (cTnT6), and cardiac troponin I (cTnI). p stands for phosphorylation. The Bruker Impact II Q-TOF allowed isotopic resolution of sarcomeric proteoforms during online RPLC-MS. (B, bottom) Boxplots display the level of relative phosphorylation of each group (n = 4). The relative abundance of the phosphorylated proteoform (P_{total}) is reported as the ratio of the peak intensity of the proteoform (mol P_i) to the summed peak intensities of all proteoforms (mol protein) of the same protein. ns means not statistically significant, * refers to a p < 0.05, and ** refers to a p < 0.01 by a Student's t test with equal variances.

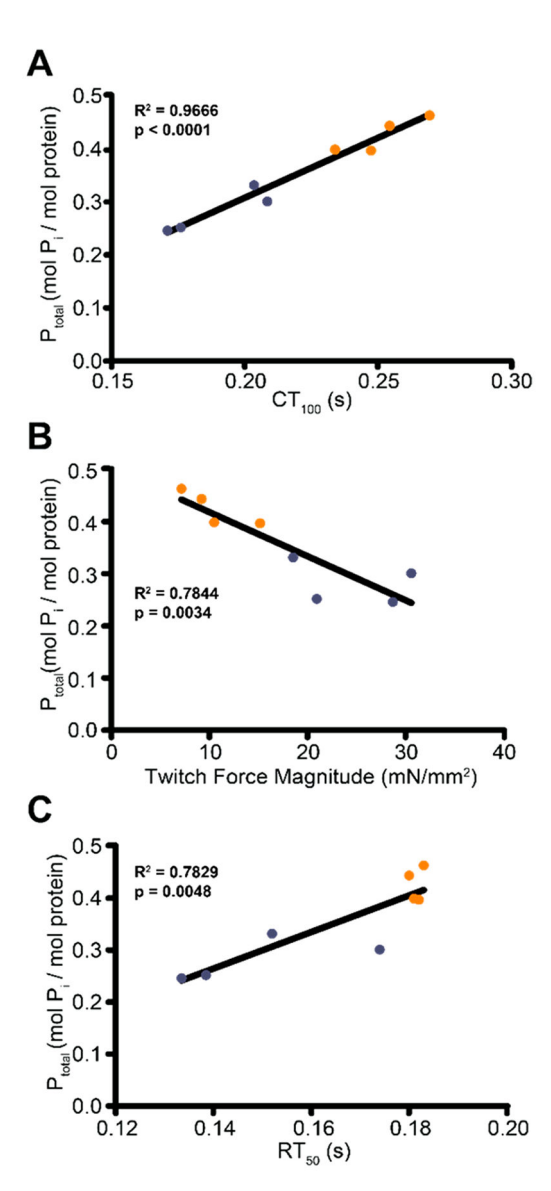


Figure 4. Correlation between functional assessments and α -Tpm phosphorylation. The relative phosphorylation levels of α -Tpm as a function of (A) CT₁₀₀, (B) twitch force magnitude, and (C) RT₅₀. The orange circles indicate data points from Day 23 hiPSC-ECTs and the blue circles indicate data points from Day 51 hiPSC-ECTs. All associations were obtained using a standard linear regression model, and R^2 and p-values are indicated in each panel.